Assembled Monolayers of Hydrophilic Particles on Water Surfaces

Geon Dae Moon,[†,§] Tae Il Lee,[†,§] Bongsoo Kim,[†] GeeSung Chae,[‡] Jinook Kim,[‡] SungHee Kim,[‡] Jae-Min Myoung,[†,*] and Unyong Jeong[†,*]

[†]Department of Materials Science and Engineering, Yonsei University, 134 Shinchon-dong, Seoul, Korea, and [‡]LG Display R&D Center, 1007, Deogeun-ri, Wollong-myeon, Paju-si, Gyeonggi-do, 413-811, Korea. [§]These authors equally contributed to this work.

ABSTRACT A facile and quick approach to prepare self-assembled monolayers of water-dispersible particles on the water surface is presented. Particle suspensions in alcohols were dropped on a water reservoir to form long-range ordered monolayers of various particles, including spherical solid particles, soft hydrogel particles, metal nanoparticles, quantum dots, nanowires, single-wall carbon nanotubes (SWCNTs), nanoplates, and nanosheets. A systematic study was conducted on the variables affecting the monolayer assembly: the solubility parameter of spreading solvents, particle concentration, zeta potential of the particles in the suspension, surface tension of the water phase, hardness of the particles, and addition of a salt in the suspension. This method requires no hydrophobic surface treatment of the particles, which is useful to exploit these monolayer films without changing the native properties of the particles. The study highlights a quick 2D colloidal assembly without cracks in the wafer scale as well as transparent conductive thin films made of SWCNTs and graphenes.

KEYWORDS: self-assembly · particle assembly · monolayer assembly · 2D assembly · colloidal assembly

Colloidal self-assembly is a general processing technique spontaneously fabricating ordered arrangement of small building blocks. The assembly is driven by various forces such as intermolecular force, electrostatic force, capillary force, or convective motion of solvents.[1−3] The key factor of the self-assembly is that the assembled building blocks are close to or at a thermodynamic equilibrium. Various types of self-assembly have been explored to produce a hexagonally closely packed 2D or 3D array for photonic crystals,[4] inverse opals,[5] and chemical sensors and biosensors.[6] Some of the simplest techniques include sedimentation and centrifugation procedures,[7−9] which are time-consuming and cause macroscopic defects in the crystalline order. Alternative methods have been tried to increase the speed of crystal formation and to enhance the colloidal ordering with a controlled thickness of the assembly. Capillary deposition,[10] spin-coating,[11] electrophoretic assembly,[12,13] convective assembly,[14] vertical deposition,[15,16] and other initiative designs[17,18] are included in this category. However, these methods often require complex configurations or long deposition time.

Since Pelton and Chibante reported the 2D arrays by an air-drying process, the drying method involving the Langmuir−Blodgett (LB) process has been used to prepare 2D colloidal crystals.[19] The solvent evaporation technique at an air−water interface has provided the basis for designing a model scheme for the quick formation of assembled colloidal crystals. There have been many studies on the monolayer assembly of particles at the air/water interface *via* the LB process. The assembly of particles with different sizes and shapes by the LB method has recently been reviewed by Yang and co-workers.[20] The LB approach employs a nonpolar liquid suspension of the particles typically using hexane or chloroform in order to trap the particles at the interface. Using a nonpolar solvent requires modification of the particle surfaces to be hydrophobic. A wide variety of nanoscale materials protected with aliphatic capping agents have been assembled into 2D monolayers using the LB technique.[21−30] Now that the environment-friendly synthesis is the current direction in solution-based particle production, most particles are obtained in polar solvents, desirably in water. Hydrophobic treatment is an additional process for the hydrophilic particles. In some materials, the hydrophilic functional groups are critical for diverse applications. For example, the oxygen functional groups such as epoxides, alcohols, and carboxylic acids in graphene oxides play a critical role in graphene-based sensors.[31] Some materials are not easy to modify or they lose their unique advantages after hydrophobic modification. Hydrogel particles (pNIPAm in this study) are difficult to turn hydrophobic, and they lose their pH- or temperature-sensitivity once they are modified. The 2D monolayer of particles with hydrophilic functional groups on a substrate allows specific

* Address correspondence to jmmyoung@yonsei.ac.kr, ujeong@yonsei.ac.kr.

Received for review June 6, 2011 and accepted October 3, 2011.

Published online October 03, 2011
10.1021/nn202733f

patterning by selective treatment, which is advantageous over the assembly of particles with hydrophobic moieties. The local chemical treatment of the particles can lead to densely multifunctionalized arrays. The use of the chemical patterning can be amplified with metal nanoparticles such as gold and silver to study optical properties and related sensor applications. Consequently, the conventional LB method is not enough to render full applicability of the monolayer formation. We need a new method that allows direct assembly of hydrophilic particles without any surface modification.

Very recently, there have been a few reports about monolayer formation of water-dispersible particles at the air/water interface by employing alcohol media instead of nonpolar solvent. McNamee *et al.* have demonstrated that TiO_2 particles (0.3−20 μm) generated stable monolayers on the water surface from an ethanol suspension of the particles.[32] Lee and coworkers have also successively created a monolayer of polystyrene (PS) particles on the water surface from an ethanol suspension.[33] In order to fully utilize the process, it is significant to understand the mechanism. Several variables are involved in the particle assembly, including the flotation/lateral capillary force, the interparticle electrostatic or van der Waals forces, and the particle−interface potential energy.

So far, a systematic study on the mechanism and variables has not been conducted, yet. This report is the first mechanistic investigation about the direct monolayer assembly of hydrophilic particles on the water surface. In this study, we found that particle aggregation in the alcohol phase at the early stage of spreading on the water surface is critical to obtain the particle monolyers. On the basis of the DLVO theory and the suggested mechanism, we investigated the effects of zeta potential, salt concentration, particle concentration, and compatibility with water of a particle suspension. We successfully demonstrated the production of monolayers from various particles including spherical SiO_2 and PS, quantum dots, Ag nanocubes, pNIPAM hydrogel particles, Te nanowires, single-wall carbon nanotubes (SWCNTs), $Co(OH)_2$ nanoplates, and graphene oxide nanosheets. The yield of the particles floating on the water surface was significantly increased by reducing the compatibility of the alcohols to water, raising particle concentration in the alcohol suspension, reducing zeta potential of the particles in the suspension, adding a salt (NaCl) in the suspension, and utilizing soft particles. The experimental results are summarized in Table 1.

RESULTS AND DISCUSSION

Scheme 1 depicts the process of the formation of an assembled monolayer on the water surface. Alcohol suspensions of particles are dropped on a water reservoir. Although alcohols are thermodynamically miscible with water, the kinetics of mixing largely depends on the viscosity and compatibility with water. Once the solvents (alcohols) are dropped on a still water surface, they quickly spread on the water surface and generate a temporary alcohol−water bilayer. Some fraction of the alcohols evaporates, and the other is gradually mixed in the water. Once the alcohol suspensions are dropped on water, the particles spread on the water surface along the alcohol flow. Ethanol's solubility parameter is slightly different from that of water ($\Delta\delta_{water-alcohol}$). It starts to mix in the water phase at the relatively early spreading stage, indicating that the particles submerge into the water phase before the particles form aggregates in the alcohol phase. Meanwhile, 1-butanol, having a large $\Delta\delta_{water-alcohol}$, can keep spreading a long distance where a thin alcohol layer is formed. The particles suspended in 1-butanol are trapped in the thin 1-butanol layer during the spreading. The concentration of the particles increases at the thin alcohol layer partly because the alcohol evaporates faster as the solvent layer becomes thinner and partly because the particles are accumulated at a long spreading distance due to the reduced moving speed. The increased particle concentration can lead to their loose aggregation, which is deformable under external shear stress. Further spreading makes the alcohol layer thinner, and the particles start to be flocculated in a two-dimensional way and are finally trapped in the air−water interface. It is well known that two similar objects floating on a liquid interface attract each other due to capillary force.[34] Since a liquid surface is supposed to be flat owing to the surface tension, the meniscus of water at the particle surface increases the energy of water. Assembly of the particles effectively decreases the deformation of the liquid surface. Once assembled at an air−water interface, the collective motion of the particles can stabilize their floating, preventing submersion in the water phase. Continuous addition of the particles from the suspension eventually leads to an assembled monolayer film of the particles on the water surface. After the monolayer of the particles covers the whole area of a container, there was no room for spreading. More drops of the particle suspension stayed at the dropping site on the water surface for a short time and submerged in the water phase with the particles. Thereafter, additional drops made the water phase opaque and did not lead to any change in the particle monolayer.

Because floating of particles depends on various conditions, calculation of the floating yield is an important step to analyze the process. With analogy to the Beer−Lambert law ($A = \varepsilon lC$), the light scattering from each particle does not interfere with each other at a very dilute particle concentration. The total scattering intensity of the suspension is linearly proportional to the particle concentration in that case. Therefore, the degree of attenuation of the incident UV−visible light

TABLE 1. Possibility of Monolayer Formation of Various Materials Used in This Study[a]

	surface functional group	EtOH solvent	IPA solvent	1-butanol solvent	NaCl addition
PS particle (500 nm)	$-OSO_3H$	x	x	o	o
PS particle (100 nm)	$-OSO_3H$	x	x	x	o
SiO_2 particle (700 nm)	$-OH$	x	x	o	o
pNIPAm particle (400 nm)	$-NH_2$	o	o	o	o
Ag nanocube (45 nm)	PVP[b] stabilized	x	x	x	o
Au nanoparticle (40 nm)	PVP stabilized	x	x	x	o
Au nanoparticle (11 nm)	CTAC stabilized	x	x	x	x
quantum dot	methacrylate	x	x	x	x
quantum dot	$-OH$	o	o	o	o
Te nanowire	negative charge of Te	x	x	o	o
SWCNT	$-NH_2$	o	o	o	o
$Co(OH)_2$ plate	$-OH$	x	o	o	o
graphene oxide	$-COOH$	x	x	o	o

[a] o: successful monolayer formation, x: lack of success. [b] PVP: poly(vinylpyrrolidone).

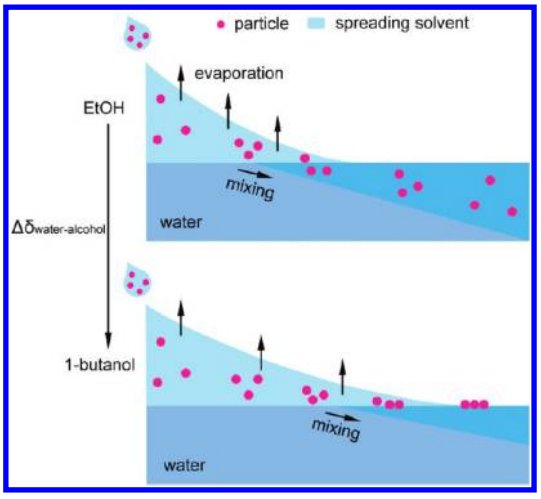

Scheme 1. Schematic illustration showing the formation of a monolayer film on the water surface. Particle suspensions in alcohol are dropped on a water reservoir. Particles suspended in spreading alcohol with a small difference in the solubility parameter ($\Delta\delta_{water-alcohol}$), *e.g*, ethanol, are easier to sink into the water phase. Particles dispersed in 1-butanol fall into flocculation at the early stage of spreading. The capillary attractive force leads to a closely packed assembly as the 1-butanol layer becomes thinner due to mixing in water and evaporation. Additional supply of the particles eventually generates a large-area monolayer of the particles

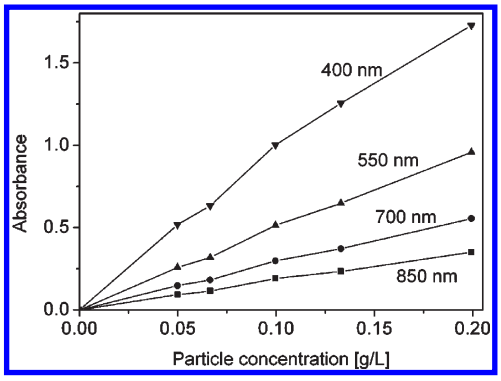

Figure 1. Standard curve showing the linear dependence of the PS particle concentration with absorbance, that is, light scattering, at different wavelengths.

caused by the particle scattering can be correlated with the particle concentration. In this study, measuring the relative fraction of the particles submerged in the water phase gives the floating yield of the particles. The floating yield (Y) of the particles can be calculated, $Y = 1 - (C/C_o) = 1 - (A/A_o)$. Here, C_o and C represent the particle concentration of the initial particle suspension and of the water phase after dropping the suspension. A_o and A are the absorbance corresponding to the concentration. We checked the reliability of the idea at various incident light wavelengths and particle concentrations. Figure 1 shows an example with polystyrene spherical particles (500 nm in diameter). The particle concentration in pure water was varied in a dilute regime, and the absorbance was measured. As shown in the figure, the absorbance linearly increased with the particle concentration at any wavelength, especially at long wavelengths at which absorbance by the PS molecules can be excluded. This linear relationship allows drawing a standard curve on the concentration of the particles; thus, the calculation of the floating yield is straightforward. The floating yields presented in the study were obtained from the calibration curves of the corresponding particles.

For a systematic study on the factors facilitating the formation of the assembled monolayer, we employed the PS particles (500 nm in diameter) dispersed in alcohols. First, the effect of compatibility of the alcohols with water was investigated. The solubility parameter difference ($\Delta\delta_{water-alcohol}$) was varied by mixing isopropyl alcohol (IPA) and 1-butanol with mixing ratios as follows: (1) 10:0, (2) 8:2, (3) 6:4, (4) 4:6, (5) 2:8, and (6) 0:10 (vol:vol). Figure 2 exhibits the difference according to the mixing ratio. When dispersed in pure ethanol or IPA, all the PS particles were submerged in

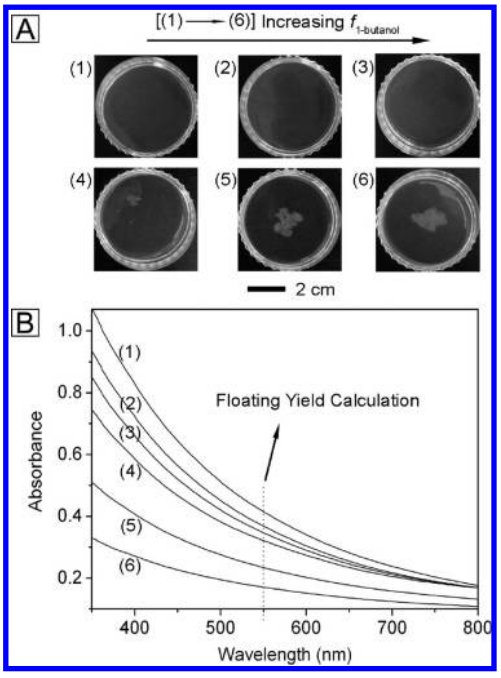

Figure 2. (A) Photographs of the area occupied by the floating PS particles (d = 500 nm) on the water surface as the volume fraction ($f_{1\text{-butanol}}$) of 1-butanol in the suspension solvent was raised. (B) UV−vis absorbance from the water phase of the corresponding samples. Absorbance at 550 nm wavelength was taken for the calculation of the floating yield.

the water phase instead of floating on the water surface. In contrast, the particles dispersed in 1-butanol readily floated. When dispersed in a solvent mixture of 1-butanol and IPA, the floating yield increased with the volume fraction of 1-butanol ($f_{butanol}$). As seen in the photographs of Figure 2A, the water surface occupied by the floating PS particles expanded as the volume fraction of 1-butanol in the suspension increased. After dropping a fixed amount of PS suspension on the water reservoir in a Petri dish, a small volume was taken from the water phase for the UV absorbance measurement. For the sample for A_o, the same amount of the alcohol suspension was directly injected in the water phase. Figure 2B exhibits the UV−vis absorbance of the water phase indicated in Figure 2A. The absorbance linearly increased with the PS particle concentration at each wavelength. Thus, any wavelength could be chosen to calculate the yield of monolayer formation. For the PS particles, we chose the absorbance at 550 nm.

Figure 3 exhibits the continuous increase in the floating yield of the PS particles as the volume fraction ($f_{butanol}$) of 1-butanol in the suspension was raised. The floating yield of the PS particles reached 60% when suspended in pure butanol. The other choice of the wavelength gave the same floating yield. The particle assembly in this study proceeds with loose aggregation in the alcohol phase near the

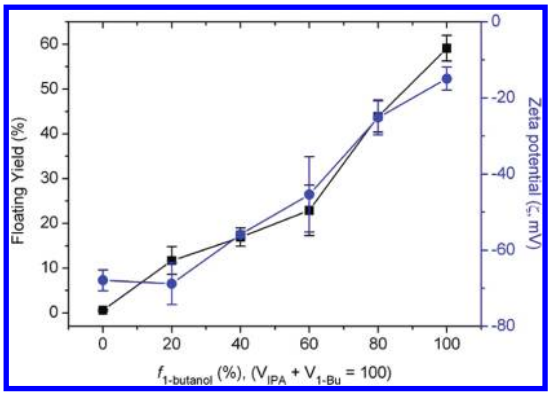

Figure 3. Floating yield (%) of the PS particles (d = 500 nm) according to the volume fraction of 1-butanol in the solvent mixture with IPA. The blue line indicates the zeta potential corresponding to the respective suspensions.

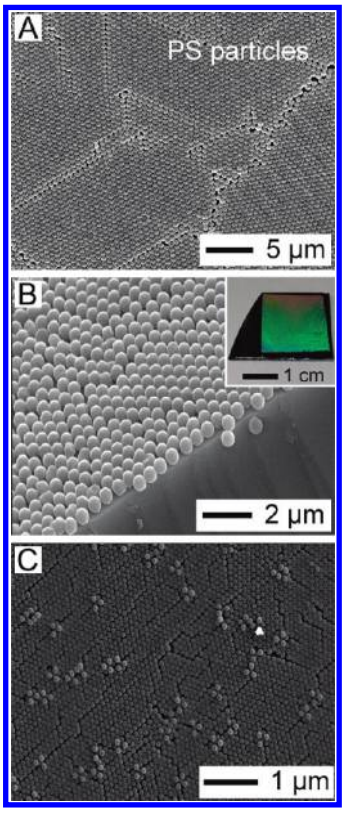

Figure 4. (A) SEM image of the assembled PS particles (d = 500 nm) after being transferred onto a Si wafer. (B) Tilted SEM image showing the monolayer of the same particles. (C) SEM image of the assembled PS particles (d = 100 nm).

dropping point of the suspension. At this point, the alcohol layer is still thick enough. The aggregation was discernible with the naked eye. The loose aggregates seem to be essential to obtain the final monolayer assembly because their collective motion can prevent submerging of the particles into the water phase. The Derjaguin−Landau−Verwey−Overbeek (DLVO) theory predicts that the electrostatic repulsion between charged spheres prevents the particles from falling into a distance of primary minimum

potential (ϕ).

$$\phi_{total} + \phi_{attractive} + \phi_{repulslive} = -Ar/(12\pi d) + 2\pi\varepsilon_0\varepsilon_r\zeta^2 \exp(-\kappa d) \quad (1)$$

where A, d, r, ε_0, ε_r, ζ, and κ^{-1} are denoted as the Hamaker constant, the particle separation, radius of the particles, the permittivity of the vacuum, relative permittivity, the zeta potential, and the Debye length, respectively. From eq 1, the repulsive force is directly proportional to the absolute value of the zeta potential, which is dependent on the species of alcohols. Since the attractive force is not sensitive to the alcohol species, a decrease in zeta potential facilitates the aggregation in the alcohol phase, thereby the final floating yield of the particles. The right axis in Figure 3 exhibits the change in zeta potential of the particles. The zeta potentials in ethanol and IPA were −70.1 and −67.9 mV, which are considered to stabilize the particles. Meanwhile, the zeta potential of the particles in 1-butanol was −14.9 mV, which is in the regime of weak stabilization. The zeta potential linearly increased as the volume fraction of 1-butanol was raised in the cosolvent. The overall tendency of the zeta potential and the floating yield was the same, as demonstrated in Figure 3, indicating the role of particle aggregation for the final monolayer assembly on the water surface.

Figure 4 displays the assembled PS particles obtained from a suspension in 1-butanol. The assembled layer on water was transferred onto a Si wafer to check. Figure 4A shows a monolayer of hexagonally close-packed particles. The dislocations are considered to take place during the evaporation of water involved in the transfer process. Figure 4B verifies the monolayer assembly of the particles. The dried PS monolayer film was iridescent in color, as shown in the photograph in the inset. PS particles with a diameter of 100 nm were also assembled into a close-packed monolayer film (Figure 4C) with a similar floating yield, which is not readily obtainable by other techniques for monolayer assembly.

From the result in Figure 3, the floating yield of the PS particles was zero when ethanol or IPA was used as the solvent. Equation 1 indicates that a decrease in the zeta potential and the Debye length can facilitate the aggregation of the particles in the alcohol phase, which is expected to enhance the formation of an assembled monolayer. An effective way to decrease both the zeta potential and the Debye length is addition of a salt that dissociates into an ionic form. We added NaCl to the PS particle suspension in IPA. The floating yield substantially increased, as seen from the photos of the water phase (Figure 5A). A clear water phase indicates most particles were floating. Figure 5B exhibits the floating yield of the PS particles as the weight ratio of NaCl increased. The floating yield substantially increased and reached a plateau value (88%) when the

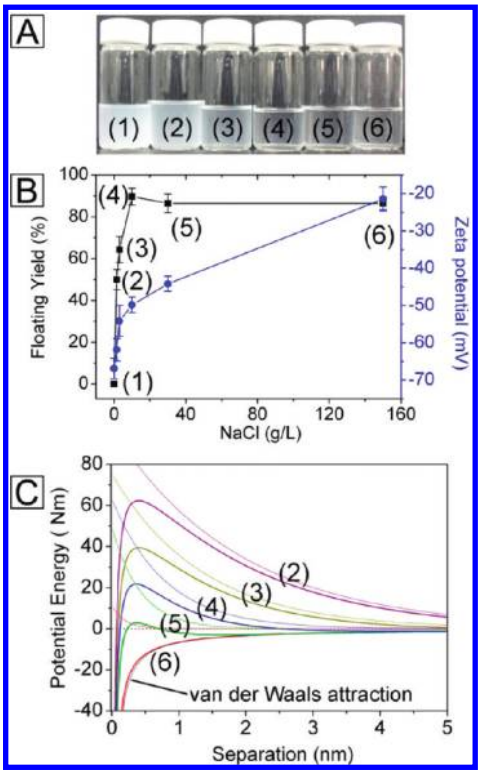

Figure 5. (A) Camera images taken for the water phase after spreading a fixed amount of the PS particle (d = 500 nm) suspension in IPA. (B) Floating yield (%) and zeta potential (blue) of PS particles in IPA with addition of salt (NaCl). (C) Change in the interaction energy between PS particles along with the particle separation. The thick lines indicate the total energy, which is the sum of attractive energy (van der Waals, black dotted line) and repulsive energy (thin lines).

concentration of NaCl was 10 g/L in the colloidal suspension. The corresponding zeta potential of the PS suspension decreased as the amount of NaCl was raised (see the blue line in Figure 5B). In a suspension of symmetric monovalent electrolyte, the Debye length (k^{-1}) of the colloids can be expressed as follows:[35]

$$k^{-1} = \sqrt{\frac{\varepsilon_o\varepsilon_r RT}{2F^2C_o}} \quad (2)$$

where ε_0 is the permittivity of free space, ε_r is the dielectric constant, R is the gas constant, F is the Faraday constant, and C_0 is the molar concentration of the electrolyte (mol/L). Figure 5C shows the change in the chemical potential according to the interparticle surface distance (d). The calculation is based on the assumptions that the Hamaker constant of the particles is not sensitive to the electrolyte concentration and NaCl in IPA is fully ionized. The energy barrier for the aggregation in the alcohol phase effectively decreased as the NaCl concentration was increased. From Figure 5B, 10 g/L of NaCl was enough to reach the maximum floating yield, which corresponds to 21.7 Nm. A 150 g/L concentration led to spontaneous flocculation of the particles without any energy barrier.

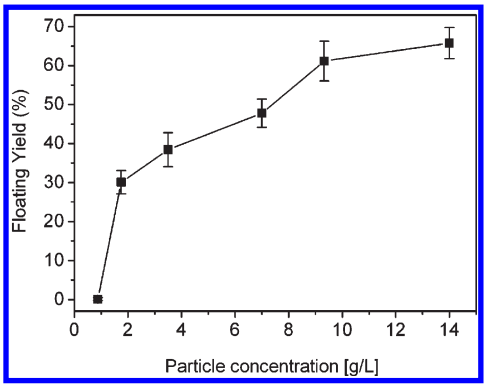

Figure 6. Floating yield (%) with respect to the concentration of PS particles (d = 500 nm) suspended in 1-butanol.

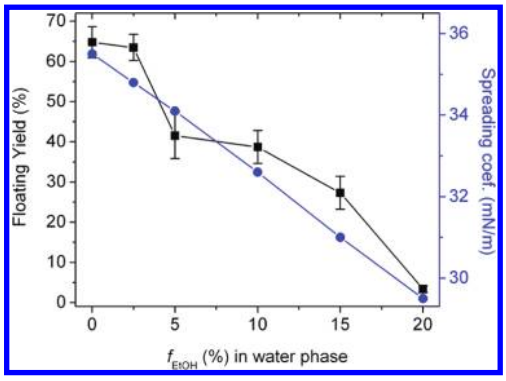

Figure 7. Floating yield (%) of PS particles (d = 500 nm) with addition of ethanol in water phase. The blue line indicates the corresponding spreading coefficients.

The loose aggregation of the particles in the alcohol phase during the initial stage of spreading was essential for the formation of monolayer assembly. The experimental observation indicates that there should be a certain critical particle concentration to be reached during the spreading process. Because the increased particle concentration (N) enhances the collision frequency (Z) between the particles with a relationship of $Z \propto N^2$, increasing the particle concentration should be an effective variable for the formation of the assembled monolayer. Figure 6 indicates that the floating yield of the PS particles dispersed in 1-butanol sharply increased with the particle concentration, which was varied from 0.88 to 14 g/L. The concentrated suspension has a higher probability of reaching the critical concentration at the early stage of spreading, thereby leading to an enhanced floating yield. In contrast, we could not observe any particle floating at low concentration (0.88 g/L).

The result in Figure 6 indicates that there is a clear limitation in the floating yield in pure 1-butanol even at very concentrated particle suspensions. The maximum floating yield is determined by the volumetric ratio between the spreading alcohol and submerging alcohol in water. Therefore, the monolayer formation should be directly related with the spreading capability of the solvent, which is denoted by the spreading coefficient (S). A liquid can spread on other media (water in this study) when the spreading coefficient is positive:[36]

$$S = \gamma_{w,a} - (\gamma_{l,w} + \gamma_{l,a}) = (\gamma_{w,a} - \gamma_{l,w}) - \gamma_{l,a} > 0 \quad (3)$$

where $\gamma_{w,a}$, $\gamma_{l,w}$, and $\gamma_{l,a}$ are the interfacial tensions between water−air, liquid−water, and liquid−air, respectively. Since the alcohols and water are thermodynamically miscible, the relative value of the spreading coefficient can determine the floating yield. In order to investigate the spreading coefficient effect, we added ethanol to the water phase to reduce the surface tension of the water phase and dropped the PS suspension dispersed in pure 1-butanol. Since both water and ethanol are polar solvents, the decrease in the interfacial tension is less than the decrease of surface tension of the water phase, thereby, $(\gamma_{w,a} - \gamma_{l,w}) > 0$ by addition of ethanol in water. The hydrophobic part of ethanol molecules[37] is considered to decrease the surface tension of water. Figure 7 shows the floating yield of the PS particles and change in spreading coefficient of the alcohol phase with respect to the volume fraction of ethanol in the water phase. The interfacial tensions were obtained by the solubility parameters of the 1-butanol and a value calucluated by a linear combination with the volume fraction of ethanol in water. The floating yield decreased to zero when the volume fraction of ethanol was 20% in the water phase.

Monodisperse spherical SiO_2 particles have been employed to fabricate planar opals or 3D photonic crystals. The Langmuir−Blodgett process has been successful in generating a monolayer of hexagonally packed silica particles, but the hydrophilic silica particles produced by the sol−gel process had to be first made hydrophobic. To demonstrate a silica particle monolayer with the close packing without any surface treatment, bare silica particles (700 nm in diameter) synthesized through the sol−gel method were dispersed in 1-butanol, and then the suspension was dropped on the water reservoir in a Petri dish. As seen in Figure 8A, the SiO_2 particle monolayer was quickly obtained on the water surface. The floating yield of the particles was 100%. The digital camera image in the inset shows the dried monolayer film transferred onto a Si wafer. The SEM image in Figure 8B confirms the monolayer hexagonal ordering of the silica particles.

As an alternative to crystals made of hard particles, crystals consisting of soft colloidal spheres can offer distinct properties that arise from the flexible polymer components.[38,39] Specific interest has been given to hydrogel particles such as poly-*N*-isopropylacrylamide (pNIPAm) due to their synthetic ease and thermoresponsive volume change. The pNIPAm particles used in this study were 400 nm in diameter, which is a

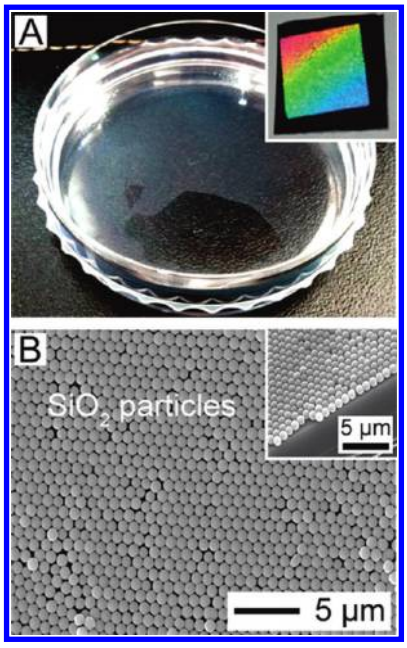

Figure 8. (A) Photograph of SiO_2 particle (d = 700 nm) monolayer on the water surface. The inset shows the film transferred onto a Si wafer. (B) SEM image showing the resultant SiO_2 monolayer film. The inset is the tilted image.

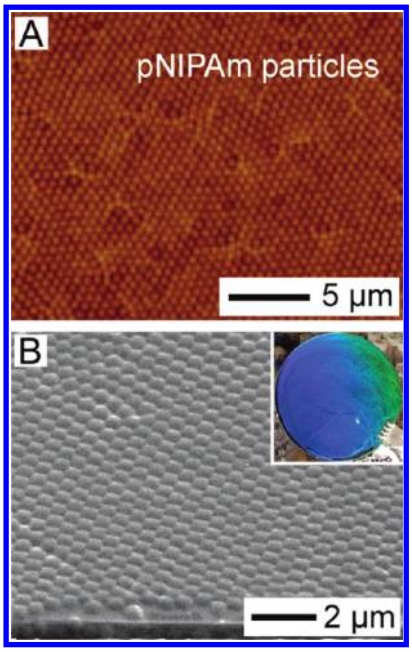

Figure 9. AFM (A) and SEM (B) images of the pNIPAm (d = 400 nm) monolayer film after transferring onto a Si wafer. The inset is a photograph of the pNIPAm monolayer transferred onto a 4 in. Si wafer.

volumetric size at room temperature in water. In contrast to other particles tested in this study, the pNIPAm particles suspended in any alcohol gave 100% floating yield. The reason is attributed to the capability of the pNIPAm particles to bear the solvent inside, which is different from solid particles such as silica or PS. The compatibility of water molecules with the pNIPAm polymer chains comes from the hydrogen bonding between water and the polymer chains, not from the surface charges. When the hydrogen bonding breaks at increased temperatures (T > 38 °C), the pNIPAm polymer chains precipitate in water. Therefore, the pNIPAm particles have poor compatibility with water as long as they are occupied with alcohols. The low compatibility is maintained until the alcohols inside the particles evaporate and water molecules fill the particles. The pNIPAm particles are considered to pack each other quickly before water molecules replace alcohol in the particles. The morphology of the dried pNIPAm monolayer film was characterized with AFM and SEM in Figure 9. The pNIPAm monolayer film on the water surface was able to be transferred onto a 4 in. Si wafer without any dislocation line. In solid particles, water accompanies the particle monolayer during the transfer process onto a new substrate. When the water evaporates, the capillary force leaves a long cleaved line in the assembly, which has been a long-term problem in the self-assembly of solid particles. In contrast, hydrogel particles can bear water molecules inside during the transfer process. This unique character allows evaporation of water molecules from the particle surfaces, not from the interparticle spaces, so that the convective force of solvent drying should be very weak. This is a potential advantage of the hydrogel particles for generating 3D colloidal photonic crystals without cracks. After complete drying, the particles were collapsed into hemispheres (500 nm in lateral diameter and 123 nm in height). The height profile of the pNIPAm particle monolayer is exhibited in the Supporting Information (Figure S1).

Long-range ordering of the particles is important for practical applications. The particles larger than 100 nm in diameter exhibited excellent low-defect hexagonal long-range ordering, as seen in the above results. Mesoscale particles had no problem with the long-range ordering as long as they are dispersible in alcohols. However, the enhanced van der Waals attraction *versus* the mass of the nanoparticles may narrow the conditions at which the nanoparticles can form a monolayer with a long-range ordering. An assembled monolayer of nanoparticles has been a widespread interest for biological and optical uses. A common route is evaporation-induced assembly on a solid substrate, which is simple, but results in low surface coverage or multilayer pile-up. The Langmuir–Blodgett method using a hydrophobic layer on the water surface has been actively employed.[20] However, the use of capping organic molecules can decrease the potential uses of the nanoparticles especially when the hydrophilic surfaces of the nanoparticles are required. We investigated the monolayer formation and ordering of various nanoparticles *via* the alcohol-assisted spreading approach.

We found that the monolayer formation and high-quality ordering of nanoparticles are sensitive to the surfactants or the capping agents, while the surface molecules in mesoscale particles did not play a critical role in the ordering. The nanoparticles stabilized with PVP successfully generated monolayers without local aggregation. With Ag nanocubes with ~40 nm side length, the formation of a monolayer with self-assembly was successful through the same process using 1-butanol (Figure 10A). As Xia and co-workers have demonstrated,[40] the Ag nanocubes can be self-assembed into specific structures by functionalizing their side faces with hydrophobic or hydrophilic self-assembled monolayers. Usually, the self-assembly of Ag nanocubes into a monolayer film requires surface treatment to exploit the mutual interaction of the adsorbed molecules unless the LB process is employed. The Ag nanocubes were synthesized *via* the polyol process in the presence of poly(vinylpyrrolidone) (PVP).[41] The nanocubes were retrieved from the solution and dispersed in 1-butanol. It is worth noting that a small amount of aqueous NaCl solution (15 g/L) had to be added into the particle suspension to enhance the floating yield. As seen in the photograph (Figure S2), the color of the Ag nanocube monolayer film reflects a collective of Ag nanocubes by close-packing, giving ~30% floating yield. Aggregation of the nanocubes was not found. The lack of excellent long-range ordering of the Ag nanocubes is simply attributed to the nonuniformity in size and shape of the particles. Normally, nanoparticles prepared in polar solvents do not show excellent size uniformity. The Au nanoparticles (~35 nm) prepared in aqueous solution in the presence of PVP showed a good monolayer without any aggregation (Figure 10B). Unfortunately, size uniformity was not good enough to expect hexagonal ordering.

When we tried to obtain a monolayer with Au nanoparticles stabilized with CTAC, spreading of a butanol suspension led to overlap of the Au nanoparticles (Figure 11A). Ligand exchange of the same Au nanoparticles by PVP in boiling water containing the PVP surfactant enabled the formation of a monolayer (Figure 11B). We conducted a similar study with quantum dots (QDs). Starting with CdSe@ZnS QDs stabilized by trioctylphosphine (TOP), we exchanged the ligand with 3-(trimethoxysilyl)propyl methacrylate. The resulting QDs were well-dispersed in alcohols, but they resulted in an aggregated layer with multiple overlaps of the particles (Figure 11C). In contrast, silica-coated CdSe@ZnS QDs (5 nm) with OH groups at the surface allowed the formation of a monolayer without particle aggregation (Figure 11D). The monolayer of the QDs on the water surface was discernible under UV illumination (Figure S2). The floating yield was almost 100%. The sensitivity of the monolayer formation to the stabilizing ligands should be related to the

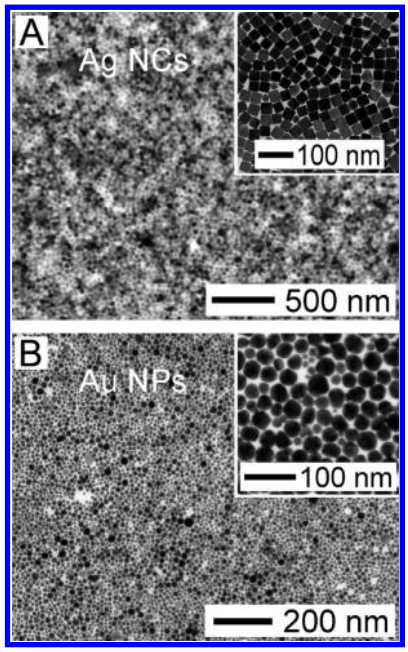

Figure 10. TEM images of the monolayers made of PVP-stabilized Ag nanocubes (A) and PVP-stabilized Au nanoparticles (B). The monolayers were directly transferred to TEM grids.

enhanced attractive force and the change in the electrostatic repulsion. Especially, the change in van der Waals attraction by replacing the capping agents needs a theoretical investigation and remains as a future study.

Recently, monolayer assembly of nanowires has been studied mainly for nanowire-based electronic devices. Langmuir–Blodgett assembly has been exploited to assemble a large-area monolayer of anisotropic building blocks.[42–45] However, surfactant modification of the nanowires to make them dispersible in hydrophobic solvents can affect their electrical and optical performances. Very recently, Yu and co-workers have demonstrated that hydrophilic ultrathin Te, Ag_2Te, and Pt nanowires could be assembled into a multilayer assembly through the LB method at an air–water interface.[29,30] However, it required a considerable amount of time to achieve high coverage in the form of a monolayer. In parallel with the spherical particles in this study, one-dimensional ultrathin Te nanowires could also be spread and assembled into a monolayer film over a large area (see the AFM image, Figure S3, for monolayer verification). As shown in the PS particles, the floating yield was very low when the nanowires were dispersed in ethanol or IPA, while 100% floating yield was achieved with 1-butanol suspension (Figure 12A,B). Whole coverage of the Petri dish took typically 40 s (see a video clip in the Supporting Information). The floating yield of the Te nanowires was effectively raised by increasing the volume fraction of 1-butanol in the IPA–butanol solvent mixture (Figure 13A) and by dissolving NaCl in an IPA suspension

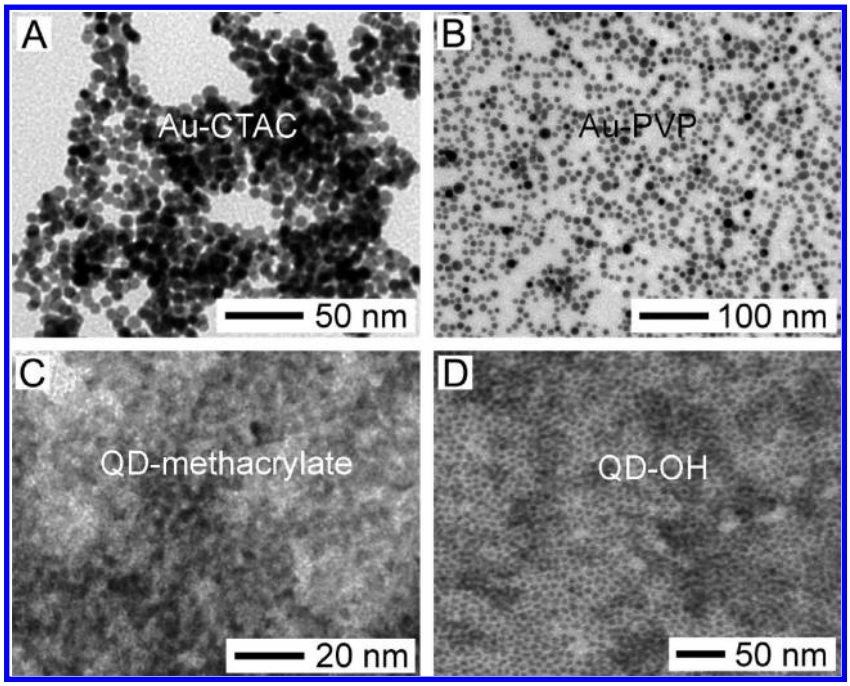

Figure 11. TEM images obtained by spreading IPA suspensions of nanoparticles: (A) CTAC-stabilized Au nanoparticles, (B) the same Au nanoparticles after ligand exchange by PVP, (C) CdSe@ZnS QDs stabilized by 3-(trimethoxysilyl)propyl methacrylate, and (D) CdSe@ZnS QDs with OH functional groups. The floating layers were directly transferred to TEM grids.

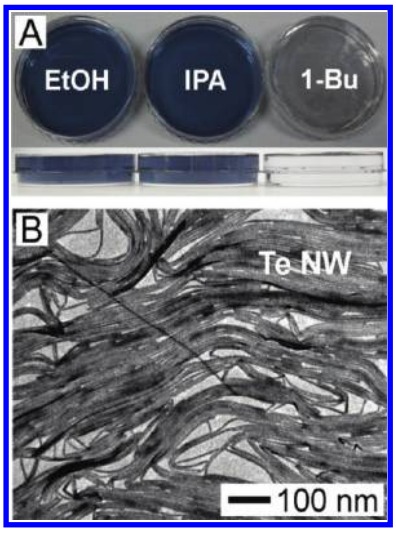

Figure 12. (A) Photographs after dropping three different alcoholic suspensions of the Te NWs on water reservoirs in Petri dishes. The bottom images are side views of each Petri dish. (B) TEM image of the Te NW monolayer made from 1-butanol suspension.

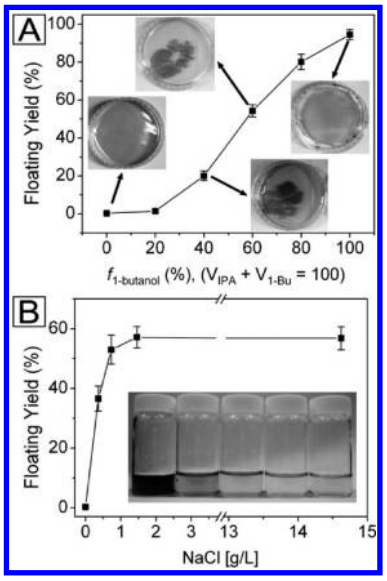

Figure 13. (A) Floating yield (%) of the Te nanowires with respect to the volume fraction of 1-butanol in the solvent mixture with IPA. (B) Floating yield (%) of of the Te nanowires with the addition of salt (NaCl).

(Figure 13B). The inset images in Figure 13B are the photographs of the water phase retrieved from a Petri dish after spreading the same amount of Te nanowire solution. It is worth noting that addition of too much NaCl in the Te nanowire alcohol suspension caused aggregation in the alcohol suspension.

In order to demonstrate the usability of the process with one-dimensional nanomaterials, we produced a monolayer of single-wall carbon nanotubes. An IPA suspension of NH_2-functionalized SWCNT (0.03 wt %) was dropped on the water surface. A thin monolayer of the SWCNT bundles was successfully obtained over the entire area of a Petri dish (see TEM and photo images in Figure 14A). There are several advantages of the process over the conventional spray coating. The coating yield through this process was 100%, which is in contrast to the typical yield by spray coating (less than 70%). The monolayer could be readily transferred to any hydrophobic substrate. Consecutive transfers of

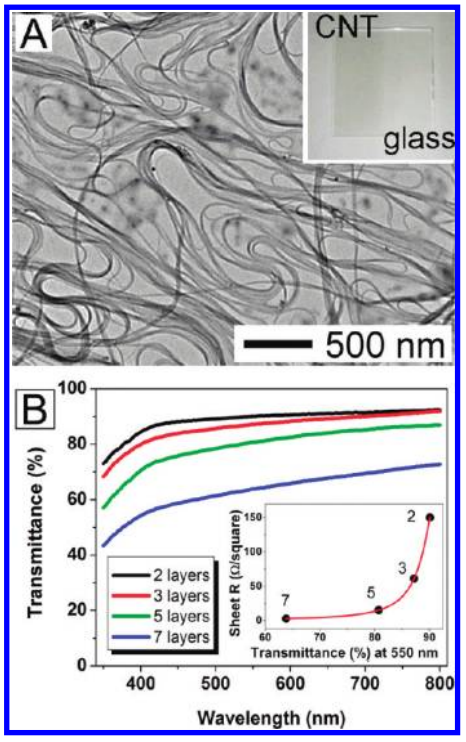

Figure 14. (A) TEM image of the single-layer SWCNT film made from IPA suspension. The inset shows the SWCNT film transferred on glass. (B) Transmittance characteristics of the multilayered SWCNT films made by multiple transfer of the SWCNT single layer to the PDMS substrate. Sheet resistance *vs* transmittance at 550 nm for each film is exhibited in the inset diagram.

the CNT monolayer allowed fine control of the thickness. The monolayer had an average topological roughness of ~20 nm (Figure S4). Multiple transfers of the monolayer led to a considerably reduced surface roughness (<60 nm), which is in contrast with the usual roughness by spray coating (300 nm). For the possible application of this thin layer as a flexible transparent conductive film (TCF), the transmittance and sheet resistance of the multilayered films on poly(dimethylsiloxane) (PDMS) were measured. After multiple transfers of the monolayer to the PDMS substrate, the multilayers were immersed in 11 M nitric acid solution for 10 min and then dried at 150 °C for 10 min. The optical and electrical characteristics of the multilayered films are exhibited in Figure 14B. The transmittance linearly decreased and the sheet resistance drastically increased as the transfer number was increased. Overall transmittance and electrical conductivities were excellent, especially at a transfer number of 3, which shows a sheet resistance below 50 Ω/cm^2 at 85% transmittance. This approach is expected to be useful in making high-quality SWCNT-based transparent conductive films as well as active channels for flexible or stretchable transistors.

Although many efforts have been devoted to assembly of nanostructured materials, the assembly of 2D nanomaterials such as nanoplates and nanosheets

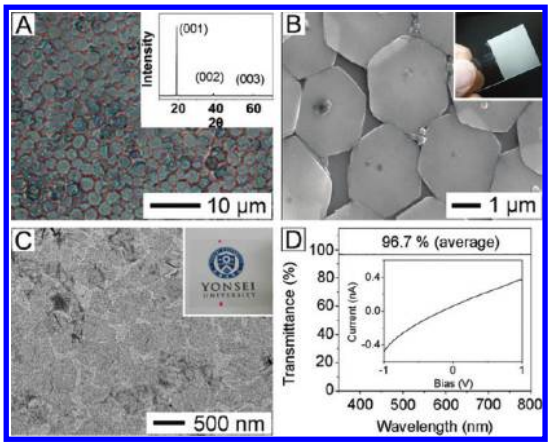

Figure 15. (A, B) Optical microscope image and SEM image of the $Co(OH)_2$ nanoplates. The inset in (A) is the XRD data from the $Co(OH)_2$ monolayer. (C) TEM image of graphene oxide monolayer film transferred onto a Cu grid. The inset shows the graphene oxide film transferred onto a glass. (D) Transmittance spectrum of the graphene oxide film and the *I*−*V* graph after reduction with N_2H_4 vapor for 10 min.

has been rarely explored. Here, we have demonstrated the monolayer self-assembly of β-$Co(OH)_2$ nanoplates and graphene oxide nanosheets floated on a water surface. The β-$Co(OH)_2$ nanoplates were dispersed in IPA as a spreading solvent, followed by dropping the suspension on the water surface. The optical microscopy image in Figure 15A shows the resultant β-$Co(OH)_2$ monolayer film transferred onto a glass slide (see the height profile in Figure S5). The inset XRD result indicates that the monolayer film has a preferential crystalline stacking on the substrate. Due to its low dimension in the *c*-axis, the β-$Co(OH)_2$ nanoplates were somewhat overlapped along their edge region (Figure 15B). Very recently, Huang and co-workers have demonstrated that graphene oxide functionalized with −COOH groups can be assembled at an air−water or oil−water interface due to its amphiphilicity.[46] In this study, the graphene oxide nanosheets functionalized with COOH were dispersed in 1-butanol and spread on the water surface. A TEM image in Figure 15C is a dried graphene oxide monolayer film transferred onto a Cu TEM grid. From the AFM analysis (see Figure S6), the film was characterized as a monolayer. The film had no aggregation or multiple stacking so that it showed a high transparency (96.7% in average) for the entire visible range, as shown in Figure 15D. After reduction with N_2H_4 vapor for 10 min, the film showed ohmic behavior in a range of −1 to 1 V (inset of Figure 15D).

CONCLUSION

In conclusion, we have demonstrated that water-dispersible particles with zero-, one-, and two-dimensional structure can be successfully spread on a water surface and form a self-assembled monolayer. The process is quick and applicable to large-area assembly.

Furthermore, no additional surface modification through hydrophobic functionalization is necessary to float particles on the water surface. We utilized the fact that alcohols initially form a transient liquid layer and finally submerge in the water phase. Particles in the alcohol phase flow along the alcohol layer and make a floating monolayer. The key to the success was enhancing the flocculation of the particles during the early stage of the spreading process. To investigate the factors affecting the monolayer film formation on the water surface, the following variables should be considered: the solubility parameter of spreading solvents, particle concentration, zeta potential of the particles in the suspension, surface tension of the water phase, hardness of the particles, and addition of a salt in the suspension. The yield of monolayer film formation could be increased *via* reducing the repulsive energy barrier: lowering the zeta potential, enhancing the density of the particles, adding salt, and increasing the surface tension of the water phase.

EXPERIMENTAL SECTION

Materials. The chemicals used in this study were telluric acid (H_6TeO_6, ≥97.5%, Aldrich), hydroxylamine (NH_2OH, 50 wt % in H_2O, Aldrich), cobalt chloride hexahydrate ($CoCl_2 \cdot 6H_2O$, 98%, Sigma-Aldrich), hexamethylenetetramine ($C_6H_{12}N_4$, HMTA, ≥99%, Sigma-Aldrich), hydrazine hydrate ($N_2H_4 \cdot xH_2O$, 55 wt %, Aldrich), L(+)-ascorbic acid ($C_6H_8O_6$, Shinyo Pure Chemicals), poly(vinyl pyrrolidone) (PVP, $M_w \approx 55\,000$, Sigma-Aldrich), silver trifluoroacetate (CF_3COOAg, ≥99.99%, Sigma-Aldrich), ethylene glycol (EG ≥99%, JT Baker), *N*-isopropylacrylamide (NIPAAm, Aldrich), *N*,*N*′-methylene bisacrylamide (MBAm, Aldrich), potassium persulfate (KPS, Aldrich), gold(III) chloride trihydrate ($HAuCl_4 \cdot 3H_2O$, Aldrich), sodium borohydride ($NaBH_4$, 99%), cetyltrimethylammonium bromide (CTAB, >99%), cetyltrimethylammonium chloride (CTAC, >98%), sodium chloride (NaCl, Aldrich), ethyl alcohol (EtOH, Sigma-Aldrich), isopropyl alcohol (IPA, Aldrich), 1-butanol (Sigma-Aldrich), tetraethyl-orthosilicate (TEOS, 99.999%, Sigma-Aldrich), and ammonium hydroxide (NH_3, 35% aqueous solution). The deionized water was obtained from an 18 MΩ (SHRO-plus DI) system. Sulfonated PS particles (d = 100 and 500 nm) were purchased from Polysciences, Inc. SWCNT dispersed in IPA and graphene oxide functionalized with COOH were purchased from Nano Solutions Co. (Korea).

Synthesis of SiO_x Particles. Silica particles (d = 700 nm) were prepared by the Stöber process.[47] Briefly, 0.67 M TEOS was added into a mixture of H_2O (4.19 M) and NH_3 (0.54 M) dissolved in 20 mL of IPA. The reaction was kept for 5 h and collected by centrifugation.

Synthesis of pNIPAm Particles. The synthesis of pNIPAm particles was carried out following the procedure of ref 48. Briefly, NIPAAm (4 g), KPS (0.12 g), and MBAm (0.16 g) were dissolved in 160 g of DI water, and this solution was agitated at 75 °C for 2 h under a nitrogen atmosphere.

Synthesis of Ag Nanocubes. Ag nanocubes were synthesized by using CF_3COOAg as a precursor according to the protocol in ref 41. Briefly, EG (50 mL) was added into a 200 mL flask and heated in an oil bath to 150 °C. The 3 mM NaHS solution (0.6 mL), 3 mM HCl (5 mL), PVP solution (20 mg/mL, 12.5 mL), and CF_3COOAg solution (282 mM, 4 mL) were added in the reaction flask in that order.

Synthesis of Au Nanoparticles. The PVP-stabilized Au nanoparticles were obtained by following the literature procedure.[49] Chloroauric acid ($HAuCl_4$, 17 mg) was dissolved in 2 mL of H_2O before it was added to the aqueous solution (45.5 mL) of PVP (0.2 g) under magnetic stirring at room temperature. The 0.2 M NaOH (1.5 mL) was added in 5 min, followed by the injection of a tetrachloro-*o*-benzoquinone solution (0.04 g in 2 mL of methanol). The reaction was allowed to proceed for 30 min, and the Au nanoparticles were collected by centrifugation. The cetyl trimethyl ammonium chloride (CTAC)-stabilized Au nanoparticles were subjected to the process reported in ref 50. Au nanoparicles (3 nm) was made by adding 0.6 mL of $NaBH_4$ solution (10 mM) into a 10 mL aqueous solution containing $HAuCl_4$ (0.25 mM) and CTAC (100 mM). The reaction was allowed to proceed for 3 h at 27 °C. Au nanoparticles (11 nm) was made by adding the above seed solution (0.3 mL) into a mixture of $HAuCl_4$ (6 mL, 0.25 mM), CTAC (6 mL), and ascorbic acid solution (4.5 mL, 0.1 M). The reaction proceeded for 1 h at room temperature. The exchange of the CTAC by PVP was conducted by refluxing the Au nanoparticles in water (5 mL) containing PVP (0.1 g) for 24 h.

Synthesis of QDs. The CdSe@ZnS QDs were prepared by following the protocol in ref 51. Briefly, a mixture of CdO (0.4 mmol), zinc acetate (4 mmol), oleic acid (5.5 mL), and 1-octadecene (20 mL) was loaded into the reaction flask and heated at 310 °C. A Se (0.4 mmol) and S (2.3 mmol) solution in 3 mL of trioctylphosphine was added into the above solution, and the mixture was allowed to react for 5 min. This oleic acid-capped CdSe@ZnS QD was further coated in the following order: undecanethiol and 11-mercapto-1-undecanol, and 3--(trimethoxysilyl)propyl methacrylate. The silane-containing methacrylate-terminated QDs were washed with methanol and chloroform. The QDs functionalized with OH groups were synthesized by following the literature procedure.[52]

Synthesis of Te Nanowires (NWs). Te nanowires with a diameter of 8−9 nm were synthesized by reducing H_6TeO_6 with NH_2OH in DI water at 95 °C for 12 h according to a procedure described in our previous report.[53]

Synthesis of β-$Co(OH)_2$ Nanoplates. The 5 mM solution of $CoCl_2 \cdot 6H_2O$ and $C_6H_{12}N_4$ was prepared in a round-bottom flask with a 200 mL solvent mixture (H_2O−EtOH, 9:1), and the temperature was raised to 90 °C for 20 min under magnetic stirring. The reaction was kept for 1 h, followed by washing with a cellulose filter (500 nm) and redispersing in EtOH.

Fabrication of Monolayer Film on a Water Surface. A clean Petri dish filled with DI water was used for the entire process of monolayer film formation. All particles in this study were dispersed in ethanol, IPA, or 1-butanol and then were dropped onto the water surface. Once the monolayer film was formed at an air−water interface, substrates (Si wafer, slide glass, PDMS) were attached onto the water surface to transfer the monolayer film.

Calculation of Floating Yield. To obtain the floating yield of the materials on the water surface, PS (d = 500 nm) and Te NW were chosen. UV−vis absorbance was employed as a parameter to calculate the floating yield of the particles. After a fixed amount of the ethanol suspension was spread on the water, the water in the bottom of the Petri dish was taken out for UV absorbance measurement. The intensity of absorbance at a specific wavelength was compared with that in which the same amount of ethanol suspension was mixed in the same volume of water. The floating yield of the PS particles was measured at 550 nm. The floating yield was the same at any wavelength. Likewise, for the yield calculation of Te NW, a wavelength (614 nm) was selected due to its unique absorption peak, whether it is a surface plasmon peak or not. To determine the effect of ion addition on the yield, different amounts of NaCl were added to the particle suspensions in IPA. Yield (%) = $[(A_{ref} - A)/A_{ref}] \times 100$.

***I*−*V* Measurement of Graphene Oxide Film.** The graphene oxide film was transferred onto a Si substrate with 20 μm spaced gold line electrodes. The film was reduced by N_2H_4 vapor for 10 min. The voltage sweep was carried out between −1 and 1 V.

Characterization. Scanning electron microscopy (SEM) images were obtained by a JEOL model JSM-6700F. Transmission electron microscopy (TEM) analysis was conducted with a JEOL model JEM-2100F operated at 200 kV. The UV−vis absorption and transmittance spectra were obtained by a JASCO V-500 UV/vis

spectrophotometer. The zeta-potential analysis was conducted by electrophoretic measurements (ELS-Z2). Topography of the monolayer was checked by AFM measurement (Dimension 3100, Digital Instrument Co). The *I*–*V* characteristic was measured by an Agilent 4156A.

Acknowledgment. This work was supported by a National Research Foundation (NRF) grant funded by the Korean Government (MEST) through the Active Polymer Center Pattern Integration (No. R11-2007-050-01004-0), the IT R&D program of MKE/KEIT [10030559, Development of next generation high performance organic/nano materials and printing process technology], and the World Class University Program (*R*32-20031). This work is also supported by the LG Display academic-industrial cooperation program.

Supporting Information Available: Video clip showing the formation of Te NW film on the water surface is provided. AFM analyses of various nanomaterials used in this study are displayed. This information is available free of charge *via* the Internet at http://pubs.acs.org.

REFERENCES AND NOTES

1. Whitesides, G. M.; Grzybowski, B. A. Self-Assembly at All Scales. *Science* **2002**, *295*, 2418–2421.
2. Whitesides, G. M.; Boncheva, M. Supramolecular Chemistry and Self-assembly Special Feature: Beyond Molecules: Self-assembly of Mesocopic and Macroscopic Components. *Proc. Natl. Acad. Sci. U. S. A.* **2002**, *99*, 4769–4777.
3. Glotzer, S. C.; Solomon, M. J. Anisotropy of Building Blocks and Their Assembly into Complex Structures. *Nat. Mater.* **2007**, *6*, 557–562.
4. Dinsmor, A. D.; Crocker, J. C.; Yodh, A. G. Self-Assembly of Colloidal Crystals. *Curr. Opin. Colloid Interface Sci.* **1998**, *3*, 5–11.
5. Xia, Y.; Gates, B.; Yin, Y.; Lu, Y. Monodispersed Colloidal Spheres: Old Materials with New Applications. *Adv. Mater.* **2000**, *12*, 693–713.
6. Holtz, J. H.; Asher, S. A. Polymerized Colloidal Crystal Hydrogel Films as Intelligent Chemical Sensing Materials. *Nature* **1997**, *389*, 829–832.
7. Pusey, P. N.; van Megen, W. Phase Behaviour of Concentrated Suspensions of Nearly Hard Colloidal Spheres. *Nature* **1986**, *320*, 340–342.
8. Davis, K. E.; Russel, W. B.; Glantschinig, W. J. Disorder-to-Order Transition in Settling Suspensions of Colloidal Silica: X-ray Measurements. *Science* **1989**, *245*, 507–510.
9. Ballato, J.; James, A. A Ceramic Photonic Crystal Temperature Sensor. *J. Am. Ceram. Soc.* **1999**, *82*, 2273–2275.
10. Li, H.-L.; Marlow, F. Solvent Effects in Colloidal Crystal Deposition. *Chem. Mater.* **2006**, *18*, 1803–1810.
11. Jiang, P.; McFarland, M. J. Large-Scale Fabrication of Wafer-Size Colloidal Crystals, Macroporous Polymers and Nanocomposites by Spin-Coating. *J. Am. Chem. Soc.* **2004**, *126*, 13778–13786.
12. Trau, M.; Saville, D. A.; Aksay, I. A. Field-Induced Layering of Colloidal Crystals. *Science* **1996**, *272*, 706–709.
13. Rogach, A. L.; Kotov, N. A.; Koktysh, D. S.; Ostrander, J. W.; Ragoisha, G. A. Electrophoretic Deposition of Latex-Based 3D Colloidal Photonic Crystals: A Technique for Rapid Production of High-Quality Opals. *Chem. Mater.* **2000**, *12*, 2721–2726.
14. Wostyn, K.; Zhao, Y.; Tee, B.; Clays, K.; Persoons, A.; De Schaetzen, G.; Hellemans, L. Optical Properties and Orientation of Arrays of Polystyrene Spheres Deposited Using Convective Self-Assembly. *J. Chem. Phys.* **2003**, *118*, 10752–10757.
15. Jiang, P.; Bertone, J. F.; Hwang, K. S.; Colvin, V. L. Single-Crystal Colloidal Multilayers of Controlled Thickness. *Chem. Mater.* **1999**, *11*, 2132–2140.
16. Li, J.; Han, Y. Optical Intensity Gradient by Colloidal Photonic Crystals with a Graded Thickness Distribution. *Langmuir* **2006**, *22*, 1885–1890.
17. Park, S. H.; Xia, Y. Assembly of Mesoscale Particles over Large Areas and Its Application in Fabricating Tunable Optical Filters. *Langmuir* **1999**, *15*, 266–273.
18. Wong, S.; Kitaev, V.; Ozin, G. A. Colloidal Crystal Films: Advances in Universality and Perfection. *J. Am. Chem. Soc.* **2003**, *125*, 15589–15598.
19. Pelton, R. H.; Chibante, P. Preparation of Aqueous Lattices with N-isopropylacrylamide. *Colloids Surf.* **1986**, *20*, 247–256.
20. Tao, A. R.; Huang, J.; Yang, P. Langmuir-Blogettry of Nanocrystals and Nanowires. *Acc. Chem. Res.* **2008**, *41*, 1662–1673.
21. Dabbousi, B. O.; Murray, C. B.; Rubner, M. F.; Bawendi, M. G. Langmuir-Blodgett Manipulation of Size-Selected CdSe Nanocrystallites. *Chem. Mater.* **1994**, *6*, 216–219.
22. Fried, T.; Shemer, G.; Markovich, G. Ordered Two-Dimensional Arrays of Ferrite Nanoparticles. *Adv. Mater.* **2001**, *13*, 1158–1161.
23. Collier, C. P.; Saykally, R. J.; Shiang, J. J.; Henrichs, S. E.; Heath, J. R. Reversible Tuning of Silver Quantum Dot Monolayers through the Metal-Insulator Transition. *Science* **1997**, *277*, 1978–1981.
24. Heath, J. R.; Knobler, C. M.; Leff, D. V. Pressure/Temperature Phase Diagrams and Superlattices of Organically Functionalized Metal Nanocrystal Monolayers: The Influence of Particle Size, Size Distribution, and Surface Passivant. *J. Phys. Chem. B* **1997**, *101*, 189–197.
25. Song, H.; Kim, F.; Connor, S.; Somorjai, G. A.; Yang, P. Pt Nanocrystals: Shape Control and Langmuir-Blodgett Monolayer Formation. *J. Phys. Chem. B* **2005**, *109*, 188–193.
26. Tao, A.; Kim, F.; Hess, C.; Goldberger, J.; He, R. R.; Sun, Y. G.; Xia, Y. N.; Yang, P. D. Langmuir-Blodgett Silver Nanowire Monolayers for Molecular Sensing Using Surface-Enhanced Raman Spectroscopy. *Nano Lett.* **2003**, *3*, 1229–1233.
27. Whang, D.; Jin, S.; Wu, Y.; Lieber, C. Large-Scale Hierarchical Organization of Nanowire Arrays for Integrated Nanosystems. *Nano Lett.* **2003**, *3*, 1255–1259.
28. Acharya, S.; Panda, A. B.; Belman, N.; Efrima, S.; Golan, Y. A Semiconductor-Nanowire Assembly of Ultrahigh Junction Density by the Langmuir-Blodgett Technique. *Adv. Mater.* **2006**, *18*, 210–213.
29. Liu, J.-W.; Zhu, J.-H.; Zhang, C.-L.; Liang, H.-W.; Yu, S.-H. Mesostructured Assemblies of Ultrathin Superlong Tellurium Nanowires and Their Photoconductivity. *J. Am. Chem. Soc.* **2010**, *132*, 8945–8952.
30. Ye, E.; Zhang, S.-Y.; Liu, S.; Han, M.-Y. Disproportionation for Growing Copper Nanowires and Their Controlled Self-Assembly Facilitated by Ligand Exchange. *Chem.—Eur. J.* **2011**, *17*, 3074–3077.
31. Robinson, J. T.; Keith Perkins, F.; Snow, E. S.; Wei, Z.; Sheehan, P. E. Reduced Graphene Oxide Molecular Sensors. *Nano Lett.* **2008**, *8*, 3137–3140.
32. McNamee, C. E.; Yamamoto, S.; Butt, H.-J.; Higashitani, K. A Straightforward Way to Form Close-Packed TiO_2 Particle Monolayers at an Air/Water Interface. *Langmuir* **2011**, *27*, 887–894.
33. Ho, C.-C.; Chen, P.-Y.; Lin, K.-H.; Juan, W.-T.; Lee, W.-L. Fabrication of Monolayer of Polymer/Nanospheres Hybrid at a Water-Air Interface. *ACS Appl. Mater. Interface* **2011**, *3*, 204–208.
34. Kralchevsky, P. A.; Nagyama, K. Capillary Forces between Colloidal Particles. *Langmuir* **1994**, *10*, 23–36.
35. Russel, W. B.; Saville, D. A.; Schowalter, W. R. *Colloidal Dispersions*; Cambridge University Press, 1989.
36. Leroux, F; Campagne, C.; Perwuelz, A.; Gengembre, L. Polypropylene Film Chemical and Physical Modifications by Dielectric Barrier Discharge Plasma Treatment at Atmospheric Pressure. *J. Colloid Interface Sci.* **2008**, *328*, 412–420.
37. Tanford, C. *The Hydrophobic Effect*; Wiley: New York, 1973.
38. Hu, Z.; Lu, X.; Gao, J. Hydrogel Opals. *Adv. Mater.* **2001**, *13*, 1708–1712.
39. McGrath, J. G.; Bock, R. D.; Cathcart, J. M.; Lyon, L. A. Self-Assembly of "Paint-On" Colloidal Crystals Using Poly(styrene-*co*-*N*-isopropylacrylamide) Spheres. *Chem. Mater.* **2007**, *19*, 1584–1591.

40. Rycenga, M.; McLellan, J. M.; Xia, Y. Controlling the Assembly of Silver Nanocubes through Selective Functionalization of Their Faces. *Adv. Mater.* **2008**, *20*, 2416–2420.
41. Zhang, Q.; Li, W.; Wen, L.-P.; Chen, J.; Xia, Y. Facile Synthesis of Ag Nanocubes of 30 to 70 nm in Edge Length with CF_3COOAg as a Precursor. *Chem.—Eur. J.* **2010**, *16*, 10234–10239.
42. Kim, F.; Kwan, S.; Akana, J.; Yang, P. Langmuir-Blodgett Nanorod Assembly. *J. Am. Chem. Soc.* **2001**, *123*, 4360–4361.
43. Patla, I.; Acharya, S.; Zeiri, L.; Israelachvili, J.; Efrima, S.; Golan, Y. Synthesis, Two-Dimensional Assembly, and Surface Pressure-Induced Coalescence of Ultranarrow PbS Nanowires. *Nano Lett.* **2007**, *7*, 1459–1462.
44. Mai, L.; Cu, Y.; Han, C.; Hu, B.; Chen, W.; Zhang, P.; Xu, L.; Guo, W.; Dai, Y. Orientated Langmuir-Blodgett Assembly of VO_2 Nanowires. *Nano Lett.* **2009**, *9*, 826–830.
45. Wang, D.; Chang, Y.-L.; Liu, Z.; Dai, H. Oxidation Resistant Germanium Nanowires: Bulk Synthesis, Long Chain Alkanethiol Functionalization, and Langmuir-Blodgett Assembly. *J. Am. Chem. Soc.* **2005**, *127*, 11871–11875.
46. Kim, J.; Cote, L. J.; Kim, F.; Yuan, W.; Shull, K. R.; Huang, J. Graphene Oxide Sheets at Interfaces. *J. Am. Chem. Soc.* **2010**, *132*, 8180–8186.
47. Hsu, W. P.; Yu, R.; Matijevic, E. Paper Whiteners: I. Titania Coated Silica. *J. Colloid Interface Sci.* **1993**, *156*, 56–65.
48. Cho, E. C.; Kim, J.-W.; Fernandez-Nieves, A.; Weitz, D. A. Highly Responsive Hydrogel Scaffolds Formed by Three-Dimensional Organization of Microgel Nanoparticles. *Nano Lett.* **2008**, *8*, 168–172.
49. Duff, D. G.; Baiker, A.; Edwards, P. P. A New Hhydrosol of Gold Clusters. 1. Formation and Particle Size Variation. *Langmuir* **1993**, *9*, 2301–2309.
50. Ma, Y.; Li, W.; Cho, E. C.; Li, Z.; Yu, T.; Zeng, J.; Xie, Z.; Xia, Y. Au@Ag Core-Shell Nanocubes with Finely Tuned and Well-Controlled Sizes, Shell Thickness, and Optical Properties. *ACS Nano* **2010**, *4*, 6725–6734.
51. Wang, T.-L; Yang, C.-H.; Shieh, Y.-T.; Yeh, A.-C. Synthesis of CdSe-poly(N-vinylcarbazole) Nanocomposite by Atom Transfer Radical Polymerization for Potential Optoelectronic Applications. *Macromol. Rapid Commun.* **2009**, *30*, 1679–1683.
52. Park, J.-J.; Prabhakaran, P.; Jang, K. K.; Lee, Y.; Lee, J.; Lee, K.; Hur, J.; Kim, J.-M.; Cho, N.; Son, Y.; Yang, D.-Y.; Lee, K.-S. Photopatternable Quantum Dots Forming Quasi-Ordered Arrays. *Nano Lett.* **2010**, *10*, 2310–2317.
53. Moon, G. D.; Ko, S.; Xia, Y.; Jeong, U. Chemical Transformations in Ultrathin Chalcogenide Nanowires. *ACS Nano* **2010**, *4*, 2307–2319.